ACS OMEGA

http://pubs.acs.org/journal/acsodf

Article

Spectroscopic Study into Lanthanide Speciation in Deep Eutectic Solvents

James T. M. Amphlett, Yunu Lee, Wonseok Yang, Dokyu Kang, Nark-Eon Sung, Jaeyeong Park, Euo Chang Jung, and Sungyeol Choi*

Cite This: *ACS Omega* 2022, 7, 921−932

Read Online

ACCESS | Metrics & More | Article Recommendations | Supporting Information

ABSTRACT: Deep eutectic solvents are a new class of green solvents that are being explored as an alternative for used nuclear fuel and critical material recycling. However, there is a paucity of knowledge regarding metal behavior in them. This paper explores the underlying chemistry of rare-earth elements in choline chloride-based deep eutectic solvents by using a multi-technique spectroscopic methodology. Results show that speciation is highly dependent on the choice of the hydrogen-bond donor. Collected EXAFS data showed Ln^{3+} coordination with ethylene glycol and urea in their respective solvents and coordination with chloride in the lactic acid system. Generalized coordination environments were determined to be $[LnL_{4-5}]$, $[LnL_{7-10}]$, and $[LnL_{5-6}]$ in the ethylene glycol, urea, and lactic acid systems, respectively. Collected UV/vis spectra for Nd^{3+} and Er^{3+} showed variations with changing solvents, showing that Ln−Cl interactions do not dominate in these systems. Luminescence studies were consistent, showing varying emission spectra with varying solvent systems. The shortest luminescent lifetimes were observed in the choline chloride−ethylene glycol deep eutectic solvent, suggesting coordination through O−H groups. Combining all collected data allowed Eu^{3+} coordination geometries to be assigned.

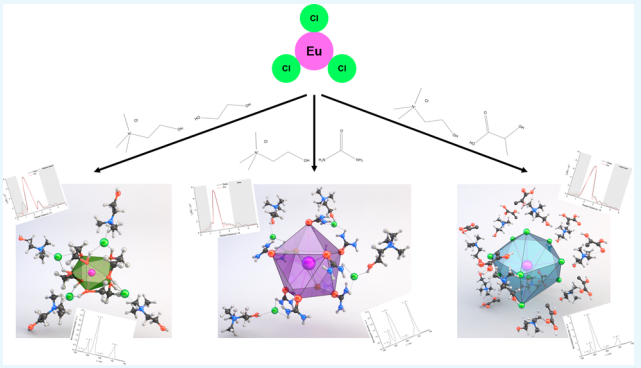

1. INTRODUCTION

Actinide and lanthanide coordination behavior in acid solutions, organic solvents, and molten salts is relatively well understood, particularly with regard to their use in used nuclear fuel treatment and critical materials recovery. However, though these solvent media are proven to be effective, their application in industrial settings is still hindered by issues such as high energy requirements, safety concerns, and cost. In an effort to overcome these issues, ionic liquids (ILs) have been explored as an alternative, due to their many beneficial properties.[1,2] However, their potential was never realized due to issues such as cost and toxicity. Deep eutectic solvents (DES's) are a new class of solvents that are now garnering attention in the metal recovery sector, as they share many of the positive attributes of ILs, while being cheaper and having the potential to be classed as green solvents with low toxicities. These solvents have the capacity to solve the issues surrounding conventional recovery processes.[3−8] DES's have many favorable characteristics for use as solvents in metal recovery processes, such as low volatility, a wide liquid range, low melting points, low/non-flammability, a large electrochemical window, low toxicity, and the potential to be tailored to specific uses based on judicious choice of constituents.[9,10] There are a number of defined types of DES's, of which this study focuses on type III, those composed of a quaternary ammonium salt (QAS) and a hydrogen-bond donor (HBD).

Rare-earth elements (REE's) are critical materials in the energy sector.[11,12] In the nuclear industry, REE's are found in relatively large amounts in used nuclear fuel. They require separation and removal to enable the recycling of nuclear materials due to their high neutron-absorption cross-sections. REE's, alongside other materials, are defined as critical due to their economic and strategic importance coupled with a substantial risk to their supply and inability to be replaced with more accessible alternatives. This necessitates the development of technologies to maintain a security of supply for them, often involving novel developments due to the use of secondary resources, such as waste electronics. Understanding of REE speciation in DES's is fundamentally important for the development of new, sustainable, and safe recovery processes. An example of this is the work conducted by Choppin and

Received: October 6, 2021
Accepted: December 8, 2021
Published: December 21, 2021

https://doi.org/10.1021/acsomega.1c05386
ACS Omega 2022, 7, 921−932

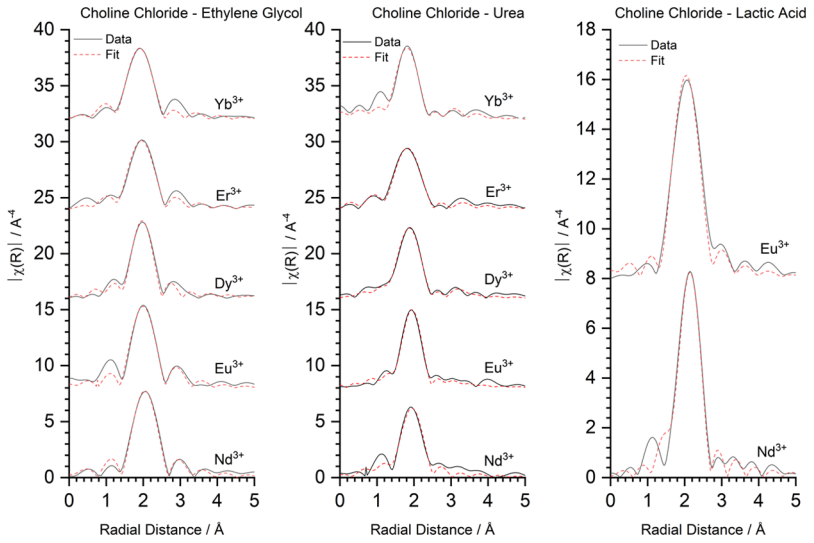

Figure 1. L_{III}-edge EXAFS spectra and fits in the R space for REEs dissolved in the choline chloride−ethylene glycol, −urea, and −lactic acid DES. Please refer to the Supporting Information for fitting windows.

Table 1. Coordination Numbers and Bond Lengths Derived From EXAFS Data Fits for REEs in Choline Chloride−Ethylene Glycol, −Urea, and −Lactic Acid DES's[a]

Ln^{3+}	ChCl−ethylene glycol				ChCl−urea				ChCl−lactic acid	
	Ln−O		Ln−C		Ln−O		Ln−C		Ln−Cl	
	N[b]	r/Å	N[c]	r/Å	N[b]	r/Å	N[c]	r/Å	N[c]	r/Å
Nd^{3+}	10/9	2.53	10	3.48	10/8	2.44			10/6	2.7
Eu^{3+}	8/9	2.5	8	3.47	9/8	2.4	9	3.54	10/5	2.62
Dy^{3+}	8/9	2.43	8	3.35	9/7	2.35	9	3.58		
Er^{3+}	8/9	2.4	8	3.94	8/7	2.31	8	3.42		
Yb^{3+}	8	2.35			8/6.5	2.26	8	3.44		

[a]Detailed EXAFS fitting parameters can be found in the Supporting Information (Tables S1−S3). [b]Numbers to the left of the slash are CNs derived from EXAFS fits. Numbers to the right of the slash are CNs based on the most-likely case based on bond distances. [c]Coordination numbers for carbon atoms are those derived from EXAFS fits, and they are likely an overestimation.

colleagues into the complexation of REE's and actinides by polyaminocarboxylate ligands, which paved the way for next-generation separation processes being developed by the nuclear industry for waste reprocessing.[13−15] In addition, the recovery of REE's is vital to address the environmental and energy challenges in other energy sectors, which are only going to be exacerbated by the growing and ever-increasingly connected global population.[12,16−21]

The REE coordination number (CN) and geometry are dominated by ligand size and therefore steric effects around the metal center. This allows for high CN complexes to form as the REEs are relatively large. In aqueous systems, nine-coordinate species of the tricapped trigonal prismatic geometry dominate, but some heavier lanthanides do exhibit eight-coordinate structures, where one of the capping water molecules has been lost.[22] The presence of other ligands in aqueous systems can result in higher CN's, such as the 12-coordinate $[Ln(NO_3)_6]^{3+}$ complexes (Ln = La, Ce, Nd, Pr).[23] Lower coordinate complexes are rare in aqueous systems but can be formed in other solvents with particularly bulky ligands.

A major challenge when using novel solvents such as DES's in metal recovery processes is the paucity of knowledge regarding metal behavior in them. Such processes often rely on differences in metal speciation between phases to drive them. This is something that is well-understood in ILs but has not enabled their scale-up progress for use in industrial separation processes as solvents,[24] a major reason for this being their cost, and questions surrounding their green credentials, particularly as they are commonly dissolved in organic solvents when they are used.[25] The green nature of DES's is heavily dependent on the chosen constituents, but it is well-established that they can be composed of "green" compounds. With this in mind, one of the largest obstacles in their use and scale-up progress for REE recovery will be this understanding of metal behavior in them. Published works that present promising REE dissolution and/or separation are unable to provide a definitive explanation of the underlying chemistry driving the process.[26−29] A comprehensive paper that details this behavior is not only needed to understand these processes but also to catalyze their scale-up progress through enabling the intelligent design of them.

In this paper, we report on the coordination environment of a range of REEs (Nd^{3+}, Eu^{3+}, Dy^{3+}, Er^{3+}, and Yb^{3+}) in a set of DES's. A multi-technique spectroscopic approach is taken, using a synergistic combination of an extended X-ray absorption fine structure (EXAFS), UV/vis absorption, and time-resolved luminescence (TRLS) spectroscopies. Choline chloride (ChCl) was selected as the QAS due to its ubiquity of use in DES's, and ethylene glycol, urea, and lactic acid were selected as as HBD's. These HBD's are historically well-represented in the literature and have been shown to exhibit similar properties when compared to other polyols, amides, or

https://doi.org/10.1021/acsomega.1c05386
ACS Omega 2022, 7, 921−932

carboxylic acids when used as an HBD. Following this, we envisage that the REE coordination environment will show similarities when switching similar HBD's, for example, ethylene glycol with glycerol, enabling the data collected here to be relevant to other type III DES's. The determined coordination environment of the REE's is discussed with reference to what we know about the molecular structure of DES's.

2. RESULTS AND DISCUSSION

2.1. EXAFS Spectroscopy. Data were collected for Nd^{3+}, Eu^{3+}, Dy^{3+}, Er^{3+}, and Yb^{3+} in the ChCl−ethylene glycol and ChCl−urea DES (Figures S1−S3). In the ChCl−lactic acid, DES data were only collected for Nd^{3+} and Eu^{3+} due to their low solubilities and thus reduced data quality. The extraction of the EXAFS function and subsequent Fourier transform gave radial distribution functions with a large peak at *ca.* 2 Å, followed by weaker peaks at greater R values (Figure 1). Fits were conducted by only considering O and Cl atoms in the first coordination sphere, with the addition of C atoms for subsequent shells if appropriate.

In the ethylene glycol DES, acceptable fits were achieved by only including oxygen atoms in the inner coordination sphere for all REE's (Tables 1, S1, Figures S4−S13). This is consistent with the expectation that Ln's coordinate with oxygen more readily than chloride. The CN was 8 for all the Ln's tested, except for Nd^{3+} which had a CN of 10. The second peak between 2.8 and 3 Å was fit with Ln-C scattering paths, producing acceptable fits for all data sets apart from Yb^{3+}. This leads to the conclusion that the coordinating ligand is ethylene glycol, as seen in this DES previously with Ni^{2+}, where Ni^{2+} is hexa-coordinated to three bidentate ethylene glycol molecules.[32] It has been reported that in this DES, the ethylene glycol is less able to disrupt the electrostatic interaction between the N^+ and Cl^- of the ChCl, meaning that the ethylene glycol is bound less strongly to the QAS.[33]

The reported Ln−O bond lengths produced from the fits in the ChCl−EG DES can be correlated with reported species in the literature. This is important as EXAFS data give much more accurate bond distances than CNs, which is of particular importance with lower quality data sets. Single-crystal X-ray diffraction data for Nd^{3+} coordinated by polyethylene glycol, Cl^-, H_2O, and NO_3^- ligands have CN's ranging from 9 to 11.[34] The average Nd−O distance to alcoholic O atoms varies from 2.45 to 2.52 Å. Our determined Nd−O distance of 2.53 Å lies just outside this range. However, when looking at a larger sample of Nd-(poly)ethylene glycol complexes, the average Nd−O distance to alcoholic O atoms varies from 2.46 to 2.58 Å. Our determined distance of 2.53 Å lies in the middle of this range. This is suggestive of a 10-coordinate complex, which would agree with a bidentate ethylene glycol ligand.

Table S11 shows a collection of Ln−O bond distances for Ln coordination complexes with (poly)ethylene glycol ligands from the Cambridge Crystallographic Data Centre (CCDC).[34−53] These data are in good agreement with our determined bond lengths for Nd^{3+}, Er^{3+}, and Yb^{3+} as 10- and 8-coordinate complexes. However, the distances for Eu^{3+} and Dy^{3+} are longer in our EXAFS fits than in the collected data when only considering the Ln−O distances for alcoholic O atoms. These longer distances may correlate with nine-coordinate complexes. In a comprehensive study of Ln−O bond distances in Ln−dimethylpropyleneurea (DMPU) complexes, Lundberg et al. used EXAFS and crystallographic data to correlate the ionic radius with CN.[54] This was done by subtracting the ionic radius of a coordinated oxygen atom (1.34 Å) from the Ln−O bond distance. Repeating this methodology with our data gives ionic radii that generally correlate well with the fit CNs but do make a definitive assignment difficult (Table S9). Assuming a bidentate ethylene glycol ligand, the data correlate. If not, a more sensible CN assignment would be nine, nine, nine, nine, and eight for Nd^{3+}, Eu^{3+}, Dy^{3+}, Er^{3+}, and Yb^{3+}, respectively.

Fits of the data in the ChCl−urea DES show some similarities with those of the ChCl−ethylene glycol DES. Acceptable fits were produced by fitting two shells to the data, the first containing O atoms and the second containing C atoms (Tables 1 and S12). The CN was more variable in this solvent, with values of 8, 9, and 10 being fit. This is consistent with a reduction in the ionic radius with increasing Ln^{3+} mass and a monodentate coordinating ligand. This is likely to be the amidic oxygen of the urea moiety, as it has been reported that the main interactions between ChCl and urea do not involve the carbonyl group, leaving it free to interact with the Ln^{3+} center.[10] It is technically possible that the alcoholic oxygen atom of the choline is involved; however, its interaction in the bulk DES structure means that the more likely coordinating moiety is urea. The Ln−O distances are shorter when urea is the HBD when compared with ethylene glycol. This is due to the monodentate nature of the urea ligand causing less steric hindrance than the bidentate ethylene glycol moiety.

Repeating the process for correlating the ionic radius with CN for the ChCl−Urea−Ln^{3+} system gives ionic radii that are lower than those from the fits (Table S10). This would give CNs of eight, eight, seven, seven, and seven for Nd^{3+}, Eu^{3+}, Dy^{3+}, Er^{3+}, and Yb^{3+}, respectively. However, this could be expected, as urea is a smaller ligand than DMPU, which is a larger, more space-demanding ligand.[54] Xiong et al. reported a nine-coordinate heteroleptic Eu^{3+} complex produced via ionothermal synthesis in the ChCl−ethyleneurea DES.[55] The three coordinating ethyleneurea ligands had Ln−O distances of 2.37, 2.38, and 2.41 Å, respectively, matching with the 2.4 Å distance produced from our EXAFS fits. This structure is encouraging as to the veracity of our fits; however, the lack of structural data for Ln^{3+} complexes associated with the DES does need to be addressed further.

A survey of the CCDC for Ln^{3+} complexes containing urea and derivatives shows a variety of CNs and Ln−O bond lengths (Table S12).[55−71,74] There are very few homoleptic complexes reported, making direct comparisons between our data and the crystal structures difficult. The homoleptic $[Dy(Urea)_8]^{3+}$ complex has an average Ln−O bond distance of 2.37 Å, slightly longer than that in our proposed $[Dy(Urea)_9]^{3+}$ complex.[67] However, the heteroleptic $[Dy(Urea)_4(H_2O)_4]^{3+}$ complex, also eight-coordinate, has an average Ln−O bond distance of 2.29 Å, which is shorter than that in our data.[72] The only other homoleptic urea complex for the Lns studied in this work in the CCDC is $[Yb(Urea)_6]^{3+}$, with a shorter average Ln−O bond length of 2.20 Å when compared with the 2.26 Å refined in this work. In contrast to this, the eight-coordinate $[Yb(propyleneurea)_8]$ complex has an average Ln−O bond distance of 2.40 Å, much longer than that proposed in our eight-coordinate structure, likely arising from steric effects.[56] The only 10-coordinate Nd^{3+} complex in the CCDC is $[Nd(Urea)_2(H_2O)(NO_3)_3]$.[73] The average $Ln-O_{Urea}$ distance in this complex is 2.44 Å, the same as in our EXAFS data. It is likely that our fitted CNs are not

https://doi.org/10.1021/acsomega.1c05386
ACS Omega 2022, 7, 921−932

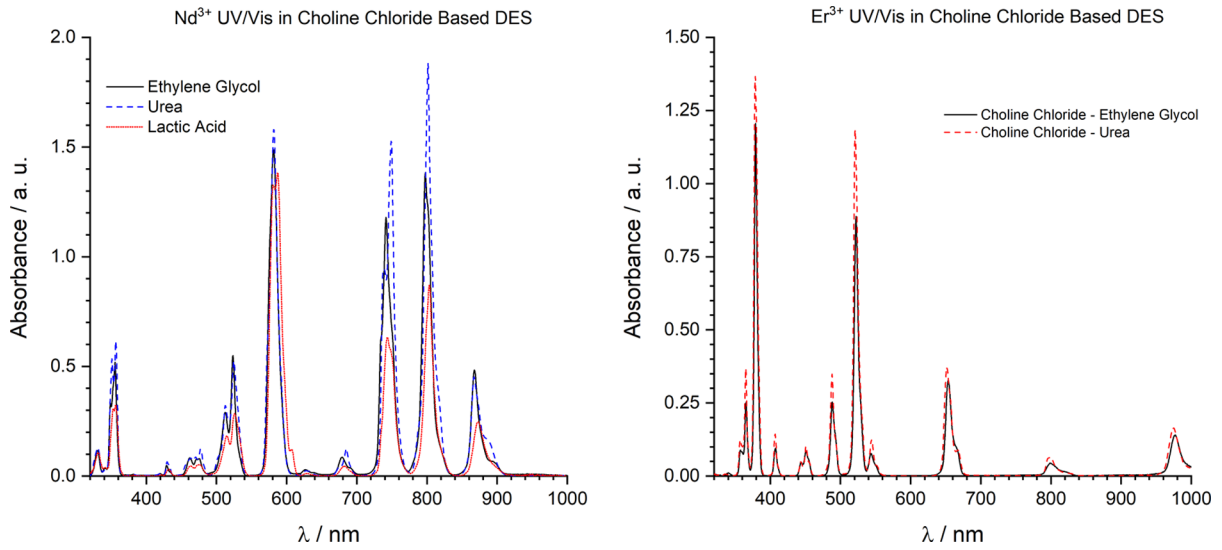

Figure 2. UV/vis spectra of Nd^{3+} and Er^{3+} in choline chloride-based DESs.

perfect, which prevents us from reporting them with confidence. However, our data do have some consistency with the previously published literature, and this report can act as a guide for what CNs to expect in such media.

Fits containing O atoms did not produce acceptable results for Nd^{3+} and Eu^{3+} in the ChCl–lactic acid DES. Instead, acceptable fits were obtained for a first coordination shell comprised of Cl^- ligands for both Ln's (Figures S4–S7, Tables 1, S3). This was unexpected, as Ln's are well known to form complexes with carboxylic acids in aqueous and non-aqueous media.[74,75] However, even though Ln's tend to prefer O-donor ligands to Cl^- ligands, this may not be true in DES's. When comparing the extracted radial distribution functions for Nd^{3+} and Eu^{3+} in each solvent, it is clear that the first peak is at a further R in the acidic DES than the other two. This means that the first coordination sphere is further away, suggestive of Cl^- atoms in that shell, as Ln–Cl distances are generally larger than Ln–O distances.

The nature of the interactions between the QAS and HBD is less understood in this solvent than in the ChCl–ethylene glycol and urea DES. However, molecular modeling has shown that there are major interactions between the lactic acid and choline moieties in the ChCl–lactic acid DES. The collected data actually suggested a repulsive interaction between the lactic acid and Cl^-.[76] These interactions result in a Cl^- ion that is less strongly interacting with the other DES molecules than in the ethylene glycol and urea cases, leaving it free to coordinate with dissolved metal species in preference to the HBD. This also goes some way in explaining the observed low solubility of Lns in the ChCl–lactic acid DES, as formation of $[LnCl_x]^{3-x}$ complexes may not be favorable.

Based on a literature survey, it seems that the fitted Ln–Cl distances for Nd and Eu correlate quite well with CN's of six and five, respectively (Table S13).[77−102] This is much lower than the fitted CN of 10 for both lanthanides. Homoleptic Nd^{3+}- and Eu^{3+}-chloro complexes tend to be six-coordinate octahedra, with average Ln–Cl distances of 2.73 and 2.69 Å, respectively. There are no examples of homoleptic Nd^{3+}- or Eu^{3+}-chloro complexes in the CCDC with a CN above six. Heteroleptic chloro complexes can show higher CNs, accompanied by an increase in the average Ln–Cl distance. Interestingly, for six-coordinate Nd^{3+}- and Eu^{3+}-chloro complexes, heteroleptic Ln–Cl distances are shorter than those for homoleptic complexes (Table S24).

Based on this, further attempts were made to include oxygen atoms in the fits, but this always resulted in unacceptable fitting parameters. There is a Nd^{3+} center coordinated by seven Cl^- ligands reported by Shan et al. with Ln–Cl distances from 2.7 to 2.9 Å, showing the high variance in the Ln–Cl distance in some Ln–chloro complexes.[103] All the Cl^- ligands in this crystal structure are bridging between two or three metal centers, which is in some ways similar to in a DES, where they will be interacting with the Ln^{3+} ions and other DES components. An 11-coordinate Eu^{3+} center in a metal–organic framework was reported with two coordinating Cl^- ligands at very short Ln–Cl distances of 2.15 and 1.92 Å, respectively.[104] This does show that highly coordinated Eu^{3+} centers can have unexpectedly short Ln–Cl distances, though this is an exception rather than a norm.

There are no homoleptic Ln-chloro complexes in the CCDC database with a CN higher than six. When considering our data and the literature, it is highly likely that our CNs are too high and that the Ln^{3+} centers are coordinated by five–six chlorides. However, with the current lack of research into the metal coordination behavior in and structure of carboxylic acid DESs, it is not possible to define the exact nature of the complexes present. This demonstrates the challenges with determining solution state structures when compared with crystal structures, as their disordered nature makes them more difficult to resolve. Solution state species can be much more variable in bond lengths and angles than crystal structures; however, it has been shown that REE coordination complexes show a good consistency between both types of structure.[22] The inclusion of La^{3+} into this work would have been valuable as it is the largest of the lanthanides and can exhibit higher CNs. Based on general trends in coordination chemistry along the lanthanide series, it is likely that the coordination structure of La^{3+} in ChCl–Urea and ChCl–lactic acid would be similar to that of Nd^{3+} as the coordinating species is monodentate. It is possible that slightly higher CNs would be seen in ChCl–ethylene glycol due to its bidentate nature. This warrants further examination, ideally including both spectroscopic and computational methodologies.

https://doi.org/10.1021/acsomega.1c05386
ACS Omega 2022, 7, 921−932

2.2. UV/Vis Absorption Spectroscopy. Interpretation of Ln^{3+} UV/vis absorption spectra is challenging, primarily owing to the Ln contraction and subsequent weak interactions of valence orbitals with those of ligating species. The observed transitions in these spectra are due to f−f electronic transitions, where the energies of the f-orbital microstates are non-degenerate due to electron repulsion, spin−orbit coupling, crystal-field effects, and the Zeeman effect.[105] These absorption bands are often quite weak, with molar extinction coefficients less than 1 L mol^{-1} cm^{-1}. Nevertheless, useful information can still be gleaned from the analysis of such spectra. Particular attention in this section will be given to Nd^{3+} and Er^{3+}, as they have easily accessible absorption spectra. Collected UV/vis absorption spectra and extracted data are shown in Figure 2 and Tables S4−S8, respectively. Oscillator strengths (f) of each transition were calculated using eq 1, where ε is the molar absorption coefficient (L mol^{-1} cm^{-1}), and ν is the wavenumber (cm^{-1}). Conversion of ε from kg mol^{-1} cm^{-1} to L mol^{-1} cm^{-1} was done using literature values for DES densities.[9,106,107]

$$f = 4.39 \times 10^{9} \int \varepsilon(\nu) \mathrm{d}\nu \quad (1)$$

Nd^{3+} UV/vis spectra show up to 16 peaks rising from the $^4I_{9/2}$ ground state, which vary in shape and intensity based on the HBD (Figure 3). This suggests that the Nd^{3+} coordination environment is different in each solvent, consistent with the EXAFS data analyses. The hypersensitive transition, $^4I_{9/2} \rightarrow {}^4G_{5/2}$ (*ca.* 580 nm), reduces in oscillator strength with the HBD in the order lactic acid > urea > ethylene glycol (Tables S4−S6). A reduction in the intensity of a hypersensitive band can be correlated with an increase in symmetry around the central Nd^{3+} ion. The $^4I_{9/2} \rightarrow {}^2G_{7/2}$ transition, which lies in the same region of the spectrum, is not visible in the urea and ethylene glycol DES but is easily discernible in the lactic acid DES.

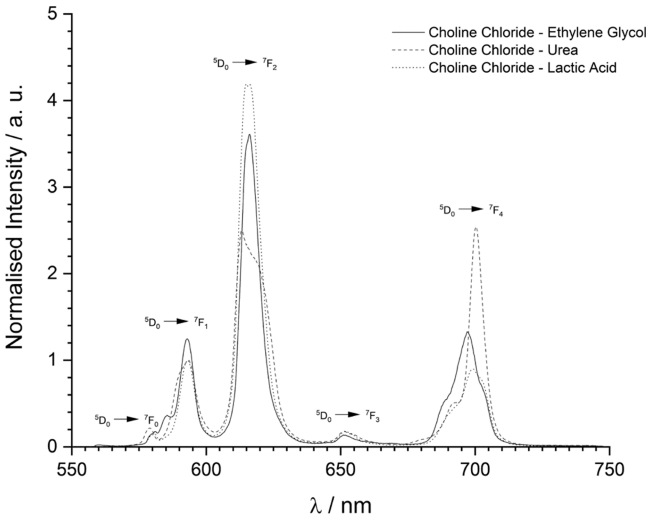

Figure 3. Luminescence spectra of $EuCl_3$ (0.02 mol kg^{-1}) dissolved in choline chloride-based DESs with ethylene glycol, urea, and lactic acid as HBDs.

The two next most intense peaks in the Nd^{3+} spectra correspond to the $^4I_{9/2} \rightarrow {}^4F_{7/2}$, $^4S_{3/2}$ (*ca.* 745 nm) and $^4I_{9/2} \rightarrow {}^4F_{5/2}$, $^2H_{9/2}$ (*ca.* 800 nm) transitions. These are not considered hypersensitive transitions, but they do show a large degree of variance between the three solvents. Of particular note is the $^4I_{9/2} \rightarrow {}^4F_{5/2}$, $^2H_{9/2}$ transition in choline chloride−urea, which is more intense than the hypersensitive $^4I_{9/2} \rightarrow {}^2G_{7/2}$ transition. This is not the case in the other two solvents. The slight changes in peak positions, intensities, and splitting are all evidence for different Nd^{3+} coordination environments in each solvent.

The UV/vis spectra of Er^{3+} are remarkably similar in both the ChCl−ethylene glycol and urea DES. In general, there are subtle differences in the peak position and intensity in each solvent, suggestive of a different coordination environment. Er^{3+} exhibits two hypersensitive transitions in absorption spectra, $^4I_{15/2} \rightarrow {}^4G_{11/2}$ (*ca.* 380 nm) and $^4I_{15/2} \rightarrow {}^2H_{11/2}$ (*ca.* 520 nm). These are by far the most intense transitions in the collected spectra, and decrease in the oscillator strength/intensity with the HBD in the order urea > ethylene glycol is seen. This is the same order as Nd^{3+}, again showing an increasing symmetry around the central Er^{3+} atom in the same order.

2.3. Luminescence Spectra. *2.3.1. Europium.* Luminescence spectra were collected for Nd^{3+}, Eu^{3+}, and Dy^{3+} in the ChCl−ethylene glycol, −urea, and −lactic acid DES. Attempts were made with solutions of Er^{3+} and Yb^{3+} but were unsuccessful due to equipment limitations. The luminescence spectra of Eu^{3+} in the choline chloride-based DES are shown in Figure 3. For comparative purposes, the spectra have been normalized as per the convention that the total integrated intensity of the $^5D_0 \rightarrow {}^7F_1$ transition is equal in each spectrum. There are obvious differences between the spectra, particularly the hypersensitive $^5D_0 \rightarrow {}^7F_2$ transition and the $^5D_0 \rightarrow {}^7F_4$ transition and more subtle differences between the other peaks. These differences are telling of different Eu^{3+} coordination environments in each DES, which agrees with the results of the EXAFS fitting.

Table 2. Peak Maxima and Relative Integrated Intensities for Luminescence Emission of Eu^{3+} Dissolved in Choline Chloride−Ethylene Glycol, −Urea, and −Lactic Acid DESs[a]

	ethylene glycol		urea		lactic acid	
transition	λ/nm	relative intensity	λ/nm	relative intensity	λ/nm	relative intensity
$^5D_0 \rightarrow {}^7F_0$	581.12	0.06	578.92	0.10	580.84	0.08
$^5D_0 \rightarrow {}^7F_1$	592.94	1.00	593.21	1.00	592.94	1.00
$^5D_0 \rightarrow {}^7F_2$	616.00	3.21	613.26	3.41	614.91	5.41
$^5D_0 \rightarrow {}^7F_3$	651.10	0.15	651.37	0.21	651.92	0.22
$^5D_0 \rightarrow {}^7F_4$	697.03	1.68	700.30	2.14	699.21	1.56

[a]The $^5D_0 \rightarrow {}^7F_1$ integrated intensities were normalized to make them equal in all spectra. Relative intensity refers to the integrated intensity of each $^5D_0 \rightarrow {}^7F_J$ transition divided by that of the $^5D_0 \rightarrow {}^7F_1$ transition.

https://doi.org/10.1021/acsomega.1c05386
ACS Omega 2022, 7, 921−932

The luminescence spectrum of Eu^{3+} in the ChCl−ethylene glycol DES is dominated by the hypersensitive $^5D_0 \rightarrow {}^7F_2$ transition, with an intensity three times that of the $^5D_0 \rightarrow {}^7F_1$ transition (Table 2). This is indicative of a geometry without an inversion center. The $^5D_0 \rightarrow {}^7F_J$ (J = 1, 3, 4) peaks are also clearly visible in the spectrum. The $^5D_0 \rightarrow {}^7F_0$ peak is slightly obscured by a shoulder on the larger $^5D_0 \rightarrow {}^7F_0$ peak, making it difficult to explicitly confirm that it is a single peak. However, the EXAFS spectroscopy data suggest the presence of one Eu^{3+} species, with eight or nine coordinating oxygen atoms. Of the possible coordination geometries, the only ones that allow a $^5D_0 \rightarrow {}^7F_0$ transition are the bicapped trigonal prism (CN = 8, C_{2v} symmetry) and the capped square antiprism (CN = 9, C_{4v} symmetry).[105,108,109] As the spectra were collected at room temperature in the liquid state, the vibronic coupling of the Eu^{3+} complex prevented the resolution of the $^{2S+1}L_J$ sublevels. Low-temperature studies would help to alleviate this problem and allow for a more confident coordination assignment, assuming no change in the coordination geometry upon freezing.

The emission spectrum of Eu^{3+} in the ChCl−urea DES shows five peaks, corresponding to the transitions $^5D_0 \rightarrow {}^7F_J$ (J = 0, 1, 2, 3, 4). The presence of the $^5D_0 \rightarrow {}^7F_0$ peak shows that the coordination geometry of the Eu^{3+} complex is C_n, C_{nv}, or C_s.[110] The EXAFS fit of eight−nine coordinating oxygen atoms would give us expected geometries of either the tricapped trigonal prism, capped square antiprism, or bicapped trigonal prism. The symmetry groups of these geometries are D_{3h}, C_{4v}, and C_{2v}, respectively. As $^5D_0 \rightarrow {}^7F_0$ transitions are not observed for D_{3h} complexes, it is logical to assign this complex to the C_{4v} or C_{2v} symmetry groups. A distorted capped square antiprismatic Eu^{3+} center was reported for the [Eu(2,2′-biphenyldicarboxylate)(NO_3)(ethyleneurea)$_3$] complex produced from the ChCl−ethyleneurea DES.[55] Additionally, as there is only one observable $^5D_0 \rightarrow {}^7F_0$ peak, we can be confident that there is only one species present, which agrees with the EXAFS fitting. The $^5D_0 \rightarrow {}^7F_1$ peak appears to be composed of two transitions, which would agree with a geometry of C_3 or higher symmetry, though it must be noted that the resolution is too low to show the individual peaks. A very intense $^5D_0 \rightarrow {}^7F_4$ peak is present in the spectrum, showing a much higher intensity than that of the $^5D_0 \rightarrow {}^7F_1$ transition. This enhanced intensity of the $^5D_0 \rightarrow {}^7F_4$ transition has been reported previously for the nine-coordinate capped square antiprismatic Eu^{3+} complex $[Eu(DOTA)(H_2O)]^-$.[111,112]

Eu^{3+} in the ChCl−lactic acid DES has the most intense $^5D_0 \rightarrow {}^7F_2$ peak in its luminescence spectrum, indicating that the Eu^{3+} ion has the lowest symmetry in this solvent. The large intensity of this hypersensitive peak is interesting, as it could be taken as evidence for a lack of an octahedral $[EuCl_6]^{3-}$ species, which exists in other high-chloride media and would fit with the Eu−Cl distance.[113] If this species was indeed present, then the spectrum would be dominated by the $^5D_0 \rightarrow {}^7F_1$ transition.[105,114−117] It is possible that the species present could be a distorted octahedron, but the $^5D_0 \rightarrow {}^7F_1$ still tends to dominate the spectra of such species.[24] A distorted capped octahedral geometry was reported for Eu^{3+} in a β-diketonate complex, which showed an intense $^5D_0 \rightarrow {}^7F_2$ transition.[21] This is an example of a high-symmetry complex showing such a transition. It is possible that there are other, non-coordinating DES constituents contributing to a large distortion of the $[EuCl_6]^{3-}$ octahedron, but we are unable to state this definitively. It is also possible that the extended H-bonding network of the DES and interactions between Cl^- and other DES constituents cause this, but this is currently speculative only. Regardless of the true nature of the Eu^{3+} coordination environment, we can confidently say that it is highly unlikely to be a 10-coordinate. The $^5D_0 \rightarrow {}^7F_0$ peak is observed, again identifying C_n, C_{nv}, or C_s as the possible symmetry groups for this complex. Interestingly, this peak in the spectrum looks like it may be composed of two separate peaks, which would indicate the presence of multiple species. However, the addition of other scattering paths to the EXAFS fit resulted in poor fits, and the luminescence lifetime (see the Supporting Information) is well-fitted with a mono-exponential function.

Structural identities of Eu^{3+} in each DES are not strictly identified from the EXAFS studies alone. The most likely coordination geometries around Eu^{3+} are the bicapped trigonal prism and capped square antiprism for the ethylene glycol and urea systems, respectively. Though a distorted octahedral geometry is suggested as most likely in the ChCl-EG system, there is more ambiguity with this than with the other solvents. DES constituents at further distances will be important in defining the true coordination structure, but these were not resolved in the collected EXAFS data. Though we have tried to define specific coordination polyhedra, it must be noted that these are not necessarily a strict reflection of reality.

2.3.2. Dysprosium and Neodymium. Luminescence spectra of Dy^{3+} are not as informative as those of Eu^{3+} with regard to the coordination geometry.[118] The spectra of Dy^{3+} in the choline chloride−ethylene glycol and −urea DES (Figure 4)

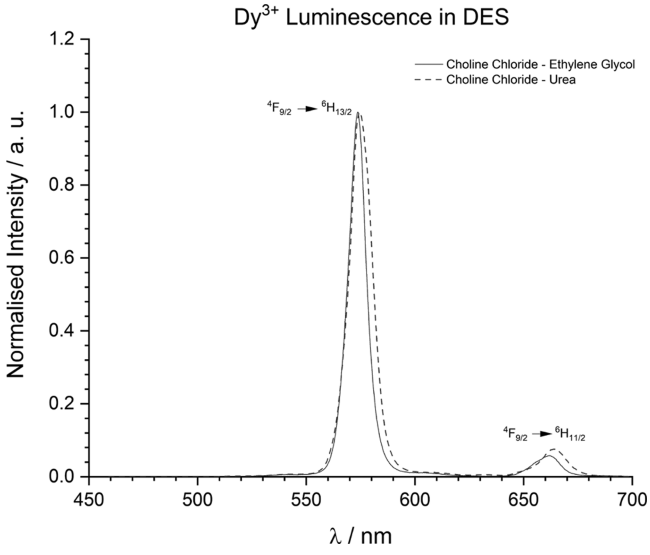

Figure 4. Luminescence spectra of $DyCl_3$ (0.02 mol kg^{-1}) dissolved in choline chloride-based DESs with ethylene glycol and urea as HBDs.

are similar, with slight differences in the peak position and intensity (Table 3). These subtle peak differences are characteristic of different Dy^{3+} coordination environments. As the EXAFS fits of Dy^{3+} and Eu^{3+} produced similar CN's in the choline chloride−ethylene glycol and −urea DES, we can say it is likely that they have the same coordination geometry. This goes some way to explaining the observed spectral differences in each DES. Only two peaks are observed for Dy^{3+} in both DES's, corresponding to the $^4F_{9/2} \rightarrow {}^6H_{13/2}$, $^6H_{11/2}$ transitions. The $^4F_{9/2} \rightarrow {}^6H_{15/2}$ transition, usually observed at

https://doi.org/10.1021/acsomega.1c05386
ACS Omega 2022, 7, 921−932

Table 3. Luminescence Transition Data for $DyCl_3$ Dissolved in Choline Chloride-Based DESs With Ethylene Glycol and Urea as HBDs

HBD	transition	λ_{max}/nm	integrated intensity
ethylene glycol	$^4F_{9/2} \rightarrow {}^6H_{13/2}$	573.6	11.35
	$^4F_{9/2} \rightarrow {}^6H_{11/2}$	661.9	0.91
urea	$^4F_{9/2} \rightarrow {}^6H_{13/2}$	574.7	13.94
	$^4F_{9/2} \rightarrow {}^6H_{11/2}$	663.8	1.27

ca. 480 nm, was not present in our collected spectra. It is not clear why this is the case, but this, combined with the intense $^4F_{9/2} \rightarrow {}^6H_{13/2}$, suggests that this medium is effective at quenching the yellow luminescence of Dy^{3+}.

Neodymium samples were excited at 355 nm, and luminescence spectra were collected by monitoring the 700−990 nm region. Unfortunately, the ICCD detector available to us is not able to detect further into the N-IR region, meaning we were unable to detect the $^4F_{3/2} \rightarrow {}^4I_{11/2}$, $^4I_{13/2}$ emission bands. The well-known $^4F_{3/2} \rightarrow {}^4I_{9/2}$ transition (*ca.* 870 nm) is present in the Nd^{3+} spectra in each DES, alongside another transition at *ca.* 800 nm, which has been assigned to the $^2H_{9/2}$, $^4F_{5/2} \rightarrow {}^4I_{9/2}$ transition, also seen in the UV/vis absorption spectra (Figure 5, Table 4). There are differences in the

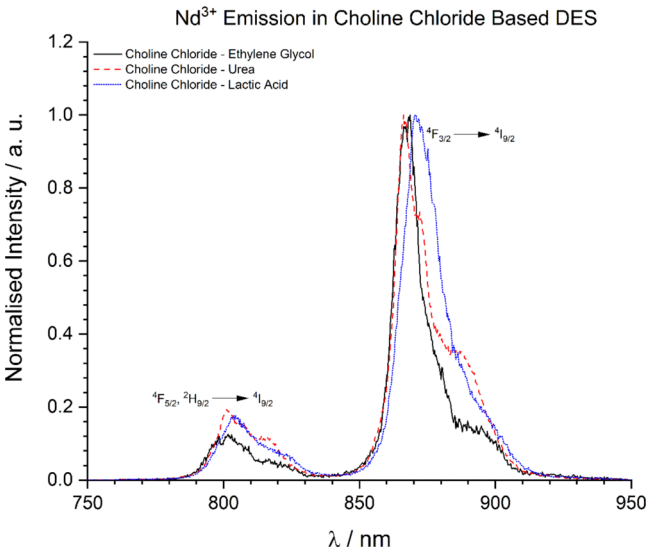

Figure 5. Luminescence spectra of $NdCl_3$ (0.02 mol kg^{-1}) dissolved in choline chloride-based DESs with ethylene glycol, urea, and lactic acid as HBDs.

Table 4. Luminescence Transition Data for $NdCl_3$ Dissolved in Choline Chloride-Based DESs with Ethylene Glycol and Urea as HBDs

HBD	transition	λ_{max}/nm	integrated intensity
ethylene glycol	$^2H_{9/2}$, $^4F_{5/2} \rightarrow {}^4I_{9/2}$	801.7	2.69
	$^4F_{3/2} \rightarrow {}^4I_{9/2}$	868.7	17.26
urea	$^2H_{9/2}$, $^4F_{5/2} \rightarrow {}^4I_{9/2}$	801.1	4.12
	$^4F_{3/2} \rightarrow {}^4I_{9/2}$	866.8	20.55
lactic acid	$^2H_{9/2}$, $^4F_{5/2} \rightarrow {}^4I_{9/2}$	803.9	3.84
	$^4F_{3/2} \rightarrow {}^4I_{9/2}$	870.3	21.55

emission spectra based on the HBD, alluding to a change of the Nd^{3+} coordination geometry, which is in agreement with both the EXAFS fits and UV/vis data. Due to our experimental limitations, it is not possible to go beyond this simplistic interpretation of the spectra.

2.4. Luminescence Lifetime. Luminescence lifetime spectra were collected for Nd^{3+} and Eu^{3+} in each of the three DES's, and spectra for Dy^{3+} were collected in the DES with ethylene glycol and urea as HBD's. Spectra were collected at concentrations of 0.01, 0.015, and 0.02 mol kg^{-1} and the fit in origin (Figures S14−S16, Table 5). All collected data were

Table 5. Luminescence Lifetimes for Ln^{3+} in Choline Chloride-Based DES. Nd^{3+}: $\lambda_{Ex.}$ = 355 nm, Monitor the $^4F_{3/2} \rightarrow {}^4I_{9/2}$ Emission. Eu^{3+}: $\lambda_{Ex.}$ = 416 nm, Monitor the $^5D_0 \rightarrow {}^7F_2$ Transition. Dy^{3+}: $\lambda_{Ex.}$ = 435 nm, Monitor the $^4F_{9/2} \rightarrow {}^6H_{13/2}$ Transition

	HBD	$[Ln^{3+}]$/mol kg^{-1}	lifetime/μs	R^2
Eu^{3+}	ethylene glycol	0.020	71.6	0.9989
		0.015	103.5	0.9979
		0.010	137.9	0.9992
	urea	0.020	467.3	0.9992
		0.015	523.6	0.9989
		0.010	617.3	0.9992
	lactic acid	0.020	308.6	0.9997
		0.015	386.1	0.9997
		0.010	427.3	0.9995
Dy^{3+}	ethylene glycol	0.020	7.2	0.9998
		0.015	7.3	0.9996
		0.010	7.3	0.9995
	urea	0.020	20.7	0.9995
		0.015	20.7	0.9996
		0.010	20.5	0.9993
Nd^{3+}	ethylene glycol	0.020	79.8×10^{-3}	0.9992
		0.015	78.4×10^{-3}	0.9995
		0.010	77.5×10^{-3}	0.9993
	urea	0.020	197.6×10^{-3}	0.9999
		0.015	198.8×10^{-3}	0.9998
		0.010	202.4×10^{-3}	0.9998
	lactic acid	0.020	157.2×10^{-3}	0.9998
		0.015	156.0×10^{-3}	0.9997
		0.010	151.5×10^{-3}	0.9989

best fit by a mono-exponential decay, indicating the presence of one species. Lifetimes for Eu^{3+} and Nd^{3+} increased according to the changing HBD in the order ethylene glycol > lactic acid > urea, with Dy^{3+} increasing in the order ethylene glycol > urea. Ln^{3+} exhibiting the shortest lifetimes in the choline chloride−ethylene glycol DES is consistent with coordination through the O−H groups of the ethylene glycol molecule. This is due to efficient luminescence quenching via O−H vibrations. These data show that the HBD has a large effect on luminescence lifetime and is indicative of a dependence of the coordination environment on the HBD, which is consistent with our discussion thus far.

The Eu^{3+} lifetime shows an inverse correlation with $[Eu^{3+}]$. This is seen in all DES's studied but is not observed for Nd^{3+} or Dy^{3+}. This may be a result of Eu^{3+} complexes reabsorbing emitted light through the inner filter effect, but there is no evidence to suggest that Eu^{3+} absorbs in the same region as its emission spectrum. However, the lifetime reductions are significantly larger when ethylene glycol is the HBD when compared with urea and lactic acid, which are similar (Table 6). This may mean that there is another quenching process

https://doi.org/10.1021/acsomega.1c05386
ACS Omega 2022, 7, 921−932

Table 6. Reduction of Eu^{3+} Luminescence Lifetime with Increasing $[Eu^{3+}]$. The Longest Lifetime was Arbitrarily Set at 100%, and all Others are Compared to This Value

	relative luminescence lifetime/%		
$[Eu^{3+}]$/mol kg^{-1}	ChCl−EG	ChCl−U	ChCl−LA
0.02	51.9	75.7	72.2
0.015	75.1	84.8	90.4
0.01	100.0	100.0	100.0

occurring, a possibility is some form of the collisional quenching process.[116] The markedly lower viscosity of choline chloride−ethylene glycol (36 cP), when compared with that of choline chloride −urea (996.8 cP) and choline chloride−lactic acid (1245.4 cP), may offer an explanation for this hypothesis.[9,106,107]

3. CONCLUSIONS

EXAFS spectroscopy has been used to determine the coordination environment of Ln^{3+} (Ln = Nd, Eu, Dy, Er, Yb) in ChCl-based DES's. These data, combined with UV/vis absorption and TRLS data, show the important relationship between the Ln^{3+} coordination environment and HBD (Table 7). All collected spectroscopic data suggest the presence of one species for each Ln^{3+} in each DES, and we have attempted to identify the complexes present based on the current understanding of the bulk molecular structure of the studied DES and literature data. The determined REE speciation illustrates the complexity of the metal behavior in DESs, whereby the intermolecular interactions between DES constituent molecules are very important in complex formation and must be considered alongside the stability of the formed complex.

The complexes determined for Ln^{3+} in ChCl−EG and ChCl−urea are consistent with the literature, based on Ln−O distances from previously published single-crystal XRD data. However, there is still some room for debate about exact CN's and coordination geometry. This is starker for the complexes in the ChCl−lactic acid DES, where Ln−Cl distances are very similar to those found in the $[LnCl_6]^{3-}$ octahedra. None of those Ln−Cl distances were measured for complexes associated with the DES in any way, where the complex intermolecular interactions could have unexpected effects. With this in mind, we recommend that future work in this area combines more spectroscopic studies of a wider range of Ln^{3+}—DES systems with computational studies. We believe that this work helps to lay the foundations of these future studies, hopefully leading to the design of DES-based separation processes which can take advantage of the relative interaction strengths between DES moieties and dissolved REE cations.

4. EXPERIMENTAL SECTION

4.1. Research Design. This work employs a set of complementary spectroscopic techniques to gain a deeper insight into the speciation of REE's in DES's than could be obtained using these techniques individually. The EXAFS spectroscopy data tell us which atoms are in the coordination sphere of the central atom and at what distance. However, this does not give us information about the specific coordination geometry. The use of UV/vis absorption and time-resolved luminescence spectroscopies fills in this gap, providing information about how complex symmetry changes are when changing the DES and enabling the elucidation of coordination geometries. A range of REE's were chosen (Nd, Eu, Dy, Er, and Yb), allowing for an understanding of how speciation changes across the row.

4.2. Reagents. $LnCl_3$ (Ln = Nd, Eu, Dy, Er, Yb, anhydrous, ≥99.9%), $LnCl_3.6H_2O$ (Ln = Nd, Eu, Dy, Er, Yb; ≥99.9%), choline chloride (98%), ethylene glycol (anhydrous, 99.8%), and urea (99.5%) were purchased from Sigma-Aldrich. L-lactic acid (anhydrous, 98%) was purchased from Alfa Aesar. All anhydrous chemicals were transferred to an Ar atmosphere glovebox [(O_2), $(H_2O) \leq 5$ ppm] for use and storage. Choline chloride and urea were dried in a vacuum oven (24 h, 80 °C) before being transferred into the glovebox.

4.3. Deep Eutectic Solvent Production. All DES production was carried out in the glovebox. Choline chloride was mixed with either ethylene glycol, urea, or lactic acid at molar ratios of 2, 2, and 1 (HBD/ChCl), respectively.[9,30] These mixtures were then heated with stirring at 60 °C until a clear homogenous liquid was formed, which typically took *ca.* 30 min. Care was taken to minimize the heating time during DES production, as the ChCl−lactic acid DES is known to degrade through an esterification reaction.[30]

4.4. EXAFS Spectroscopy Measurements. EXAFS spectroscopy measurements were performed at the Pohang Accelerator Laboratory (PAL) using beamlines 6D, 7D, and 8C. Data were collected at room temperature in the fluorescence mode, using the L-III edge of Nd, Eu, Dy, Er, and Yb. $LnCl_3$ salts were dissolved in the DES in a glovebox [(Ln^{3+}) = 0.1 mol kg^{-1}] before being transferred into sealed sample holders for analysis. Collected spectra were processed using the Demeter software suite.[31] Specifically, normalization was carried out using the Athena software package, and subsequent data fits were carried out using the FEFF database in the Artemis software package. The coordination number for each fitted shell was set, and the amplitude reduction factor was allowed to refine based on the model.

4.5. UV/Vis Spectroscopy. Stock solutions of $NdCl_3$ and $ErCl_3$ were made in choline chloride−ethylene glycol and −urea DES's [(Ln^{3+}) = 0.2 mol kg^{-1}]. A stock solution of $NdCl_3$ was also made in choline chloride−lactic acid [(Ln^{3+}) = 0.06 mol kg^{-1}]. Aliquots of each stock were taken and diluted appropriately for measurement. All sample preparation was

Table 7. Identified Metal Species for REEs (Nd, Eu, Dy, Er, and Yb) in Choline Chloride-Based DES with Ethylene Glycol, Urea, and Lactic Acid as HBDs

	identified Ln^{3+} species				
HBD	Nd	Eu	Dy	Er	Yb
ethylene glycol	$[Nd(HBD)_{4.5-5}]$	$[Eu(HBD)_{4-4.5}]$	$[Dy(HBD)_{4-4.5}]$	$[Er(HBD)_{4-4.5}]$	$[Yb(HBD)_4]$
urea	$[Nd(HBD)_{8-10}]$	$[Eu(HBD)_{8-9}]$	$[Dy(HBD)_{7-9}]$	$[Er(HBD)_{7-8}]$	$[Er(HBD)_{7-8}]$
lactic acid	$[NdCl_6]$	$[EuCl_{6-5}]$			

https://doi.org/10.1021/acsomega.1c05386
ACS Omega 2022, 7, 921−932

done in the glovebox, and samples were only removed from the glovebox for measurement in lidded cuvettes. UV/vis absorption spectroscopy data were recorded using a Zeiss MCS 600 spectrometer.

4.6. Time-Resolved Luminescence Spectroscopy. Luminescence emission and lifetime were collected at room temperature for $LnCl_3$ (Ln = Nd, Eu, Dy) in the studied DES [(Ln^{3+}) = 0.01, 0.015, 0.02 mol kg^{-1}]. Excitation wavelengths of 416 nm (pulse energy of 1.6 mJ), 453 nm (1.54 mJ), and 355 nm (4.9 mJ) were used for Eu, Dy, and Nd, respectively. A pulsed Nd:YAG laser at 355 nm (Continuum, Surelite) and a wavelength-tunable optical parametric oscillator (OPO, OPOTEK, Vibrant B) were used for TRLS studies. The laser pulse energy was measured using an energy meter (Coherent, EPM 2000 with a J25LP-MB detector), and the gated intensified charge-coupled device (ICCD, Andor, DH-720/18U-03 iStar 720D) was used to collect the time-resolved luminescence spectra. A more detailed explanation of the TRLS experiments is included in the Supporting Information.

■ ASSOCIATED CONTENT

Supporting Information

The Supporting Information is available free of charge at https://pubs.acs.org/doi/10.1021/acsomega.1c05386.

Plotted EXAFS data, plotted TRLFS data, EXAFS fitting data, data extracted from UV/vis spectra, tabulated Ln-ligand CNs, consolidated crystallographic data from the CCDC, and detailed TRLFS experimental description (PDF)

■ AUTHOR INFORMATION

Corresponding Author

Sungyeol Choi − *Department of Nuclear Engineering, Seoul National University, Seoul 08826, Republic of Korea;* orcid.org/0000-0002-7164-8491; Email: choisys7@snu.ac.kr

Authors

James T. M. Amphlett − *Nuclear and Quantum Engineering Department, Korea Advanced Institute of Science and Technology (KAIST), Daejeon 34141, Republic of Korea;* Present Address: Seaborg Technologies, Titangade 11, 2200, Copenhagen, Denmark

Yunu Lee − *Nuclear and Quantum Engineering Department, Korea Advanced Institute of Science and Technology (KAIST), Daejeon 34141, Republic of Korea;* orcid.org/0000-0003-1422-9466

Wonseok Yang − *Nuclear and Quantum Engineering Department, Korea Advanced Institute of Science and Technology (KAIST), Daejeon 34141, Republic of Korea*

Dokyu Kang − *Nuclear and Quantum Engineering Department, Korea Advanced Institute of Science and Technology (KAIST), Daejeon 34141, Republic of Korea*

Nark-Eon Sung − *Pohang Accelerator Laboratory, POSTECH, Pohang 37673, Republic of Korea*

Jaeyeong Park − *School of Mechanical, Aerospace and Nuclear Engineering, Ulsan National Institute of Science and Technology, Ulsan 44919, Republic of Korea*

Euo Chang Jung − *Nuclear Chemistry Research Team, Korea Atomic Energy Research Institute, Daejeon 34057, Republic of Korea*

Complete contact information is available at: https://pubs.acs.org/10.1021/acsomega.1c05386

Funding

This work was supported through the National Research Foundation of Korea (NRF) funded by the Ministry of Science and ICT directly (grant number: NRF-2020R1A2C2013078) and via the Brain Pool Program (grant number: NRF-2018H1D3A1A01074757).

Notes

The authors declare no competing financial interest.

■ ACKNOWLEDGMENTS

The authors would like to thank members of the KAIST nuclear fuel cycle group for their support throughout this work and Dr. Louise Natrajan for her insightful discussion about luminescence data acquisition. This work was supported by the Pohang Accelerator Laboratory (PAL) in Pohang, Republic of Korea.

■ REFERENCES

(1) Sun, X.; Luo, H.; Dai, S. Ionic Liquids-Based Extraction: A Promising Strategy for the Advanced Nuclear Fuel Cycle. *Chem. Rev.* **2012**, *112*, 2100−2128.

(2) Cocalia, V.; Gutowski, K.; Rogers, R. The Coordination Chemistry of Actinides in Ionic Liquids: A Review of Experiment and Simulation. *Coord. Chem. Rev.* **2006**, *250*, 755−764.

(3) Gupta, R.; Gamare, J.; Gupta, S. K.; Kumar, S. S. Direct Dissolution of Uranium Oxides in Deep Eutectic Solvent: An Insight Using Electrochemical and Luminescence Study. *J. Mol. Struct.* **2020**, *1215*, 128266.

(4) Gupta, R.; Vats, B.; Pandey, A. K.; Sharma, M. K.; Sahu, P.; Yadav, A. K.; Ali, S. M.; Kannan, S. Insight into Speciation and Electrochemistry of Uranyl Ions in Deep Eutectic Solvents. *J. Phys. Chem. B* **2020**, *124*, 181−189.

(5) Abbott, A. P.; Capper, G.; Davies, D. L.; Rasheed, R. K.; Tambyrajah, V. Novel Solvent Properties of Choline Chloride/Urea Mixtures. *Chem. Commun.* **2003**, *9*, 70−71.

(6) Albler, F.-J.; Bica, K.; Foreman, M. R. S.; Holgersson, S.; Tyumentsev, M. S. A Comparison of Two Methods of Recovering Cobalt from a Deep Eutectic Solvent: Implications for Battery Recycling. *J. Clean. Prod.* **2017**, *167*, 806−814.

(7) Van Osch, D. J. G. P.; Parmentier, D.; Dietz, C. H. J. T.; Van Den Bruinhorst, A.; Tuinier, R.; Kroon, M. C. Removal of Alkali and Transition Metal Ions from Water with Hydrophobic Deep Eutectic Solvents. *Chem. Commun.* **2016**, *52*, 11987−11990.

(8) Tran, M. K.; Rodrigues, M.-T. F.; Kato, K.; Babu, G.; Ajayan, P. M. Deep Eutectic Solvents for Cathode Recycling of Li-Ion Batteries. *Nat. Energy* **2019**, *4*, 339−345.

(9) Smith, E. L.; Abbott, A. P.; Ryder, K. S. Deep Eutectic Solvents (DESs) and Their Applications. *Chem. Rev.* **2014**, *114*, 11060−11082.

(10) Silva, L. P.; Araújo, C. F.; Abranches, D. O.; Melle-Franco, M.; Martins, M. A. R.; Nolasco, M. M.; Ribeiro-Claro, P. J. A.; Pinho, S. P.; Coutinho, J. A. P. What a Difference a Methyl Group Makes-Probing Choline-Urea Molecular Interactions through Urea Structure Modification. *Phys. Chem. Chem. Phys.* **2019**, *21*, 18278−18289.

(11) *Critical Raw Materials Resilience: Charting a Path towards Greater Security and Sustainability*; Brussels, 2021.

(12) Bobba, S.; Carrara, S.; Huisman, J.; Mathieux, F.; Pavel, C. *Critical Materials for Strategic Technologies and Sectors in the EU − A Foresight Study*, 2020.

(13) Gritmon, T. F.; Goedken, M. P.; Choppin, G. R. The Complexation of Lanthanides by Aminocarboxylate Ligands-I. Stability Constants. *J. Inorg. Nucl. Chem.* **1977**, *39*, 2021−2023.

(14) Choppin, G. R.; Williams, K. R. The Kinetics of Exchange between Americium(III) and Europium Ethylenediaminetetraacetate. *J. Inorg. Nucl. Chem.* **1973**, *35*, 4255−4269.

(15) Gelis, A. V.; Lumetta, G. J. Actinide Lanthanide Separation Process-ALSEP. *Ind. Eng. Chem. Res.* **2014**, *53*, 1624−1631.
(16) Blengini, G. A.; Latunussa, C. E. L.; Eynard, U.; Torres de Matos, C.; Wittmer, D.; Georgitzikis, K.; Pavel, C.; Carrara, S.; Mancini, L.; Unguru, M.; Blagoeva, D.; Mathieux, F.; Pennington, D. *Study on the EU's List of Critical Raw Materials*, 2020.
(17) Government, U. S. *Final List of Critical Minerals 2018*; Department of the Interior, U.S.A., 2018; Vol. *83*.
(18) Dutta, T.; Kim, K.-H.; Uchimiya, M.; Kwon, E. E.; Jeon, B.-H.; Deep, A.; Yun, S.-T. Global Demand for Rare Earth Resources and Strategies for Green Mining. *Environ. Res.* **2016**, *150*, 182−190.
(19) Mancheri, N. A.; Sprecher, B.; Bailey, G.; Ge, J.; Tukker, A. Effect of Chinese Policies on Rare Earth Supply Chain Resilience. *Resour. Conserv. Recycl.* **2019**, *142*, 101−112.
(20) Anastas, P.; Eghbali, N. Green Chemistry: Principles and Practice. *Chem. Soc. Rev.* **2010**, *39*, 301−312.
(21) Jyothi, R. K.; Thenepalli, T.; Ahn, J. W.; Parhi, P. K.; Chung, K. W.; Lee, J.-Y. Review of Rare Earth Elements Recovery from Secondary Resources for Clean Energy Technologies: Grand Opportunities to Create Wealth from Waste. *J. Clean. Prod.* **2020**, *267*, 122048.
(22) Persson, I.; D'Angelo, P.; De Panfilis, S.; Sandström, M.; Eriksson, L. Hydration of Lanthanoid(III) Ions in Aqueous Solution and Crystalline Hydrates Studied by EXAFS Spectroscopy and Crystallography: The Myth of the "Gadolinium Break. *Chem.—Eur. J.* **2008**, *14*, 3056−3066.
(23) Cotton, S. A. Establishing Coordination Numbers for the Lanthanides in Simple Complexes. *Compt. Rendus Chem.* **2005**, *8*, 129−145.
(24) Binnemans, K. Lanthanides and Actinides in Ionic Liquids. *Chem. Rev.* **2007**, *107*, 2592−2614.
(25) Ranke, J.; Stolte, S.; Störmann, R.; Arning, J.; Jastorff, B. Design of Sustainable Chemical ProductsThe Example of Ionic Liquids. *Chem. Rev.* **2007**, *107*, 2183−2206.
(26) Pateli, I. M.; Abbott, A. P.; Binnemans, K.; Rodriguez Rodriguez, N. Recovery of Yttrium and Europium from Spent Fluorescent Lamps Using Pure Levulinic Acid and the Deep Eutectic Solvent Levulinic Acid-Choline Chloride. *RSC Adv.* **2020**, *10*, 28879−28890.
(27) Entezari-Zarandi, A.; Larachi, F. Selective Dissolution of Rare-Earth Element Carbonates in Deep Eutectic Solvents. *J. Rare Earths* **2019**, *37*, 528−533.
(28) Foreman, M. R. S. Progress towards a Process for the Recycling of Nickel Metal Hydride Electric Cells Using a Deep Eutectic Solvent. *Cogent Chem.* **2016**, *2*, 1139289.
(29) Liu, C.; Yan, Q.; Zhang, X.; Lei, L.; Xiao, C. Efficient Recovery of End-of-Life Ndfeb Permanent Magnets by Selective Leaching with Deep Eutectic Solvents. *Environ. Sci. Technol.* **2020**, *54*, 10370−10379.
(30) Rodriguez Rodriguez, N.; Van Den Bruinhorst, A.; Kollau, L. J. B. M.; Kroon, M. C.; Binnemans, K. Degradation of Deep-Eutectic Solvents Based on Choline Chloride and Carboxylic Acids. *ACS Sustainable Chem. Eng.* **2019**, *7*, 11521−11528.
(31) Ravel, B.; Newville, M. ATHENA,ARTEMIS,HEPHAESTUS: data analysis for X-ray absorption spectroscopy usingIFEFFIT. *J. Synchrotron Radiat.* **2005**, *12*, 537−541.
(32) Hartley, J. M.; Ip, C.-M.; Forrest, G. C. H.; Singh, K.; Gurman, S. J.; Ryder, K. S.; Abbott, A. P.; Frisch, G. EXAFS Study into the Speciation of Metal Salts Dissolved in Ionic Liquids and Deep Eutectic Solvents. *Inorg. Chem.* **2014**, *53*, 6280−6288.
(33) Stefanovic, R.; Ludwig, M.; Webber, G. B.; Atkin, R.; Page, A. J. Nanostructure, Hydrogen Bonding and Rheology in Choline Chloride Deep Eutectic Solvents as a Function of the Hydrogen Bond Donor. *Phys. Chem. Chem. Phys.* **2017**, *19*, 3297−3306.
(34) Rogers, R. D.; Rollins, A. N.; Henry, R. F.; Murdoch, J. S.; Etzenhouser, R. D.; Huggins, S. E.; Nunez, L. Direct Comparison of the Preparation and Structural Features of Crown Ether and Polyethylene Glycol Complexes of NdCl3·6H2O. *Inorg. Chem.* **1991**, *30*, 4946−4954.
(35) Kusrini, E.; Saleh, M. I.; Lecomte, C. Coordination of Ce(III) and Nd(III) with Pentaethylene Glycol in the Presence of Picrate Anion: Spectroscopic and X-Ray Structural Studies. *Spectrochim. Acta, Part A* **2009**, *74*, 120−126.
(36) Hirashima, Y.; Tsutsui, T.; Shiokawa, J. X-Ray Crystal Structure Analysis of Neodymium Nitrate Complex with Triethylene Glycol. *Chem. Lett.* **1982**, *11*, 1405.
(37) Hirashima, Y.; Tsutsui, T.; Shiokawa, J. X-Ray Crystal Structure of Neodymium Nitrate Complex with Tetraethylene Glycol. *Chem. Lett.* **1981**, *10*, 1501−1504.
(38) Rogers, R. D.; Voss, E. J.; Etzenhouser, R. D. F-Element/Crown Ether Complexes. 17. Synthetic and Structural Survey of Lanthanide Chloride Triethylene Glycol Complexes. *Inorg. Chem.* **1988**, *27*, 533−542.
(39) Hines, C. C.; Bauer, C. B.; Rogers, R. D. Lanthanide Polyether Complexation Chemistry: The Interaction of Hydrated Lanthanide-(Iii) Nitrate Salts with an Acyclic 18-Crown-6 Analog, Pentaethylene Glycol. *New J. Chem.* **2007**, *31*, 762−769.
(40) Rogers, R. D.; Etzenhouser, R. D.; Murdoch, J. S.; Reyes, E. Macrocycle Complexation Chemistry. 35.1 Survey of the Complexation of the Open Chain 15-Crown-5 Analogue Tetraethylene Glycol with the Lanthanide Chlorides. *Inorg. Chem.* **1991**, *30*, 1445−1455.
(41) Kusrini, E.; Saleh, M. I.; Adnan, R.; Fun, H. K.; Adhha Abdullah, M. A. Ternary Complexes of Neodymium(III) and Samarium(III) Picrate Triethylene Glycol: Structural, Spectroscopic, and Photoluminescent Properties. *J. Inclusion Phenom. Macrocyclic Chem.* **2012**, *74*, 425−436.
(42) Peng, G.; Zhang, Y.-Y.; Li, Z.-Y. Effect of Coordination Environment on the Magnetic Relaxation of Mononuclear DyIII Field-Induced Single Molecule Magnets. *Inorg. Chem. Commun.* **2017**, *77*, 40−43.
(43) Kusrini, E.; Saleh, M. I. Luminescence and Structural Studies of Yttrium and Heavier Lanthanide-Picrate Complexes with Pentaethylene Glycol. *Inorg. Chim. Acta* **2009**, *362*, 4025−4030.
(44) Rogers, R. D.; Rollins, A. N.; Etzenhouser, R. D.; Voss, E. J.; Bauer, C. B. Structural Investigation into the Steric Control of Polyether Complexation in the Lanthanide Series: Macrocyclic 18-Crown-6 versus Acyclic Pentaethylene Glycol. *Inorg. Chem.* **1993**, *32*, 3451−3462.
(45) Kusrini, E.; Saleh, M. I.; Adnan, R.; Yulizar, Y.; Sha Shiong, N.; Fun, H. K.; Adhha Abdullah, M. A.; Mamat, M.; Za'aba, N. K.; Abd. Majid, W. H. Structural, Optical and Electrical Properties of Europium Picrate Tetraethylene Glycol Complex as Emissive Material for OLED. *J. Lumin.* **2012**, *132*, 91−99.
(46) Rogers, R. D.; Etzenhouser, R. D. Structure of [DyCl 3 (Triethylene Glycol)].18-Crown-6. *Acta Crystallogr., Sect. C: Cryst. Struct. Commun.* **1988**, *44*, 1533−1535.
(47) Rogers, R. D.; Etzenhouser, R. D.; Murdoch, J. S. Triethylene Glycol Complexes of the Early Lanthanide(III) Chlorides. *Inorg. Chim. Acta* **1992**, *196*, 73−79.
(48) Rogers, R. D. *CCDC 1587129: Experimental Crystal Structure Determination; Cambridge Crystal Structural Database*, 2017.
(49) Rogers, R. D. *CCDC 1587130: Experimental Crystal Structure Determination; Cambridge Crystal Structural Database*, 2017.
(50) Rogers, R. D. *CCDC 1824377: Experimental Crystal Structure Determination; Cambridge Crystal Structural Database*, 2018.
(51) Rogers, R. D. *CCDC 1824376: Experimental Crystal Structure Determination; Cambridge Crystal Structural Database*, 2018.
(52) Forsellini, E.; Casellato, U.; Tomat, G. Rinitrato-(O, O')-(Triethylene Gly Col)Europium(Ill), Eu(N O 3)3(C 6H 14 O 4)*. *Acta Crystallogr., Sect. C: Cryst. Struct. Commun.* **1984**, *40*, 795−797.
(53) Lu, T.; Ji, L.; Tan, M.; Kaibei, Y. A Structural Change between the Complexes of Praseodymium and Neodymium Nitrates with (Z) -. *Polyhedron* **1997**, *16*, 1149−1156.
(54) Lundberg, D.; Persson, I.; Eriksson, L.; D'Angelo, P.; De Panfilis, S. Structural Study of the N,N′-Dimethylpropyleneurea Solvated Lanthanoid(III) Ions in Solution and Solid State with an Analysis of the Ionic Radii of Lanthanoid(III) Ions. *Inorg. Chem.* **2010**, *49*, 4420−4432.

https://doi.org/10.1021/acsomega.1c05386
ACS Omega 2022, 7, 921−932

(55) Xiong, W. L.; Wang, Y. L.; Liu, Q. Y.; Yao, Y.; Xiong, L. H. Two Lanthanide Coordination Polymers with Helical Chain Structures Synthesized Ionothermally from a Deep-Eutectic Solvent: Syntheses, Structures and Luminescence. *Inorg. Chem. Commun.* **2014**, *46*, 282−284.
(56) Nishiura, M.; Okano, N.; Imamoto, T. *X-Ray Structural Analyses of Rare Earth Trifluoromethanesulfonate Complexes Bearing Urea Derivatives*; Bulletin of the Chemical Society of Japan, 1999, pp 1793−1801. DOI: 10.1246/bcsj.72.1793.
(57) Golubev, D. V.; Albov, D. V.; Kravchenko, V. V.; Alikberova, L. Y.; Rukk, N. S. *CCDC 750828: Experimental Crystal Structure Determination; Cambridge Crystal Structural Database*, 2011.
(58) Romanenko, G. V.; Podberezskaya, N. V.; Bakakin, V. V.; Sakharova, Y. G.; Bogodukhova, T. I. Experimental Crystal Structure Determination. *Zh. Strukt. Khim.* **1985**, *26*, 103.
(59) Alikberova, L. Y.; Albov, D. V.; Golubev, D. V.; Kravchenko, V. V.; Rukk, N. S. Experimental Crystal Structure Determination. *Koord. khimiia* **2008**, *34*, 549.
(60) Alikberova, L. Y.; Albov, D. V.; Kibalnikov, P. S.; Zaitseva, M. G.; Kravchenko, V. V.; Fedorova, G. A.; Rukk, N. S. Experimental Crystal Structure Determination. *Koord. khimiia* **2011**, *37*, 635.
(61) Alikberova, L. Y.; Albov, D. V.; Kibalnikov, P. S.; Zaitseva, M. G.; Kravchenko, V. V.; Fedorova, G. A.; Rukk, N. S. Experimental Crystal Structure Determination. *Koord. khimiia* **2012**, *38*, 460.
(62) Liu, Q. Y.; Li, Y. L.; Xiong, W. L.; Wang, Y. L.; Luo, F.; Liu, C. M.; Chen, L. L. Urothermal Synthesis of Mononuclear Lanthanide Compounds: Slow Magnetization Relaxation Observed in Dy Analogue. *Cryst. Eng. Commun.* **2014**, *16*, 585−590.
(63) Mattos, M. C.; Surcouf, E.; Mornon, J. P. Structure Cristalline Du Perehlorate d'Aqua Hexakis(Dimrthyl-l,3 Urre) Erbium(Ill) { El'[C O(NH C H 3)2]6 H 20}(CLO 4)3. *Acta Crystallogr., Sect. B: Struct. Crystallogr. Cryst. Chem.* **1977**, *33*, 1855−1861.
(64) Alikberova, L. Y.; Lyssenko, K. A.; Rukk, N. S.; Mytareva, A. I. Carbamide-Containing Complexes of Lanthanides: Competition of Hydrogen Bonding and Polyiodide Ion Formation. *Mendeleev Commun.* **2011**, *21*, 204−205.
(65) Wu, A. Q.; Guo, G. H.; Yang, C.; Zheng, F. K.; Liu, X.; Guo, G. C.; Huang, J. S.; Dong, Z. C.; Takano, Y. Extended Structures and Magnetic Properties of Lanthanide-Copper Complexes with Picolinic Acids as Bridging Ligands. *Eur. J. Inorg. Chem.* **2005**, *10*, 1947−1954.
(66) Diamantopoulou, E.; Papaefstathiou, G. S.; Terzis, A.; Raptopoulou, C. P.; Desseyn, H. O.; Perlepes, S. P. Hydrogen Bonded Networks Based on Lanthanide(III) Complexes of N,N′-Dimethylurea (DMU): Preparation, Characterisation, and Crystal Structures of [Nd(DMU)6][NdCl6] and [Nd(NO3)3(DMU)3]. *Polyhedron* **2003**, *22*, 825−835.
(67) Savinkina, E. V.; Golubev, D. V.; Grigoriev, M. S.; Albov, D. V. Iodine Networks in Polyiodides of M(III) Urea Complexes: Crystal Structures of [V(Ur)6][I3]3 and [Dy(Ur) 8][IS][I3]2[I2]. *Polyhedron* **2013**, *54*, 140−146.
(68) Zhang, J.; Wu, T.; Chen, S.; Feng, P.; Bu, X. Versatile Structure-Directing Roles of Deep-Eutectic Solvents and Their Implication in the Generation of Porosity and Open Metal Sites for Gas Storage. *Angew. Chem., Int. Ed.* **2009**, *48*, 3486−3490.
(69) Kirillova, N. I.; Gusev, A. I.; Furmanova, N. G.; Soboleva, L. V.; Edgorbekov, D. E. Experimental Crystal Structure Determination. *Kristallografiya* **1983**, *28*, 886.
(70) Alikberova, L. Y.; Albov, D. V.; Golubev, D. V.; Kravchenko, V. V.; Rukk, N. S. *CCDC 672704: Experimental Crystal Structure Determination; Cambridge Crystal Structural Database*, 2008.
(71) Albov, D. V.; Alikberova, L. Y. *CCDC 1061334: Experimental Crystal Structure Determination; Cambridge Crystal Structural Database*, 2017.
(72) Golubev, D. V.; Albov, D. V.; Kravchenko, V. V.; Alikberova, L. Y.; Rukk, N. S. Structural Features of the Crystalline Iodide Complexes of Some Rare-Earth Elements with Carbamide and Acetamide. *Russ. J. Coord. Chem. Khimiya* **2010**, *36*, 820−827.
(73) Sadikov, G. G.; Sergienko, V. S.; Porai-Koshits, M. A.; Suleimanov, K. H. Experimental Crystal Structure Determination. *Koord. Khimiia* **1987**, *13*, 689.
(74) Nockemann, P.; Thijs, B.; Lunstroot, K.; Parac-Voet, T. N.; Görller-Walrand, C.; Binnemans, K.; Van Hecke, K.; Van Meervelt, L.; Nikitenko, S.; Daniels, J.; Hennig, C.; Van Deun, R. Speciation of Rare-Earth Metal Complexes in Ionic Liquids: A Multiple-Technique Approach. *Chem.—Eur. J.* **2009**, *15*, 1449−1461.
(75) Tian, G.; Martin, L. R.; Rao, L. Complexation of Lactate with Neodymium(III) and Europium(III) at Variable Temperatures: Studies by Potentiometry, Microcalorimetry, Optical Absorption, and Luminescence Spectroscopy. *Inorg. Chem.* **2010**, *49*, 10598−10605.
(76) Altamash, T.; Nasser, M. S.; Elhamarnah, Y.; Magzoub, M.; Ullah, R.; Anaya, B.; Aparicio, S.; Atilhan, M. Gas Solubility and Rheological Behavior of Natural Deep Eutectic Solvents (NADES) via Combined Experimental and Molecular Simulation Techniques. *ChemistrySelect* **2017**, *2*, 7278−7295.
(77) Han, Y.; Lin, C.; Meng, Q.; Dai, F.; Sykes, A. G.; Berry, M. T.; May, P. S. (BMI)3LnCl6 Crystals as Models for the Coordination Environment of LnCl3 (Ln = Sm, Eu, Dy, Er, Yb) in 1-Butyl-3-Methylimidazolium Chloride Ionic-Liquid Solution. *Inorg. Chem.* **2014**, *53*, 5494−5501.
(78) Löble, M. W.; Keith, J. M.; Altman, A. B.; Stieber, S. C. E.; Batista, E. R.; Boland, K. S.; Conradson, S. D.; Clark, D. L.; Lezama Pacheco, J.; Kozimor, S. A.; Martin, R. L.; Minasian, S. G.; Olson, A. C.; Scott, B. L.; Shuh, D. K.; Tyliszczak, T.; Wilkerson, M. P.; Zehnder, R. A. Covalency in Lanthanides. An X-Ray Absorption Spectroscopy and Density Functional Theory Study of LnCl6x- (x = 3, 2). *J. Am. Chem. Soc.* **2015**, *137*, 2506−2523.
(79) Tamborino, F.; Bielec, P.; Hoch, C. Redetermination of [EuCl2(H2O)6]Cl. *Acta Crystallogr., Sect. E: Struct. Rep. Online* **2014**, *70*, i27.
(80) Wang, Z. G.; Bian, Q. Q.; Huang, B. M.; Liu, T.; Liu, S. M. Experimental Crystal Structure Determination. *Huaxue Yanjiu Yu Yingyong* **2012**, *24*, 916.
(81) Alvarez-Vicente, J.; Dandil, S.; Banerjee, D.; Gunaratne, H. Q. N.; Gray, S.; Felton, S.; Srinivasan, G.; Kaczmarek, A. M.; Van Deun, R.; Nockemann, P. Easily Accessible Rare-Earth-Containing Phosphonium Room-Temperature Ionic Liquids: EXAFS, Luminescence, and Magnetic Properties. *J. Phys. Chem. B* **2016**, *120*, 5301−5311.
(82) De Bettencourt-Dias, A.; Beeler, R. M.; Zimmerman, J. R. Secondary-Sphere Chlorolanthanide(III) Complexes with a 1,3,5-Triazine-Based Ligand Supported by Anion-Ï, Ï-Ï, and Hydrogen-Bonding Interactions. *Inorg. Chem.* **2020**, *59*, 151−160.
(83) Kong, D. Y.; Wang, S. W.; Zhu, Q.; Xie, Y. Y.; Huang, X. Y. Experimental Crystal Structure Determination. *Jiegou Huaxue* **1998**, *17*, 61.
(84) Becker, A.; Urland, W. Synthese, Kristallstruktur Und Magnetismus von [(CH3)2NH2][NdCl4(H2O)2]. *Z. Anorg. Allg. Chem.* **1999**, *625*, 217−220.
(85) Mackenstedt, D.; Urland, W. Synthese Und Bau Yon (4-Picolinium),[LnCl,(H,O),]C1 (Ln = Eu, Ho). *Z. Anorg. Allg. Chem.* **1993**, *619*, 1393−1396.
(86) Urland, W.; Schwanitz-schiiller, U. Structural Relationship of [(C6H,),As]NdCL. 8 H20 and NdC13. 6 H,O : Transition from a Three-Dimensional to a Layer Structure. *Angew. Chem., Int. Ed.* **1983**, *22*, 1009−1010.
(87) Runge, P.; Schulze, M.; Urland, W. Darstellung Und Kristallstruktur von (CH3NH3)8[NdCI,] [NdC14(H20)2]2C. *Z. Anorg. Allg. Chem.* **1991**, *592*, 115−120.
(88) Hines, C. C.; Cordes, D. B.; Griffin, S. T.; Watts, S. I.; Cocalia, V. A.; Rogers, R. D. Flexible Coordination Environments of Lanthanide Complexes Grown from Chloride-Based Ionic Liquids. *New J. Chem.* **2008**, *32*, 872−877.
(89) Reuter, G.; Frenzen, G. The Thermal Dehydration of Cs3LnCl6 · 3H2O to Cs3LnCl6 (Ln = La-Nd) and Their Crystal Structures. *J. Solid State Chem.* **1995**, *116*, 329−334.

https://doi.org/10.1021/acsomega.1c05386
ACS Omega 2022, 7, 921−932

(90) Ananyev, I. V.; Nelyubina, Y. V.; Puntus, L. N.; Lyssenko, K. A.; Eremenko, I. L. Peculiarities of Metal—Ligand Bonding in Europium Trinitrate Complexes: A Viewpoint of Comparative Charge Density Analysis in Crystals. *Russ. Chem. Bull.* **2016**, *65*, 1178−1188.
(91) Bravard, F.; Bretonnière, Y.; Wietzke, R.; Gateau, C.; Mazzanti, M.; Delangle, P.; Pécaut, J. Solid-State and Solution Properties of Cationic Lanthanide Complexes of a New Neutral Heptadentate N4O3 Tripodal Ligand. *Inorg. Chem.* **2003**, *42*, 7978−7989.
(92) Semenova, L. I.; Skelton, B. W.; White, A. H. Structural Systematics of Rare Earth Complexes. XXII 4-Methylpyridinium Salts of Diverse Complex Aqua/Chloro/Lanthanoid(III) Species. *Z. Anorg. Allg. Chem.* **2006**, *632*, 2405−2418.
(93) Evans, W. J.; Shreeve, J. L.; Ziller, J. W.; Doedens, R. J. Structural Diversity in Solvated Lanthanide Halide Complexes. *Inorg. Chem.* **1995**, *34*, 576−585.
(94) Lin, S. H.; Dong, Z. C.; Huang, J. S.; Zhang, Q. E.; Lu, J. X. Structure of Trichlorotetrakis(Tetrahydrofuran)Europium(III). *Acta Crystallogr., Sect. C: Struct. Chem.* **1991**, *47*, 426−427.
(95) Petriček, S. Syntheses and Crystal Structures of Anionic Lanthanide Chloride Complexes [(CH3)2NH2][LnCl4(HMPA) 2] (Ln = La, Nd) and [(CH3)2NH 2]4[LnCl6]Cl (Ln = Nd, Sm, Eu). *Acta Chim. Slov.* **2005**, *52*, 398−403.
(96) Hallfeldt, J. *CCDC 225124: Experimental Crystal Structure Determination*; Cambridge Cryst. Struct. Database, 2004.
(97) Yao, H. S.; Zhang, J. G.; Fan, X.; Shen, Q.; Zhang, Y. Experimental Crystal Structure Determination. *Jiegou Huaxue* **2007**, *26*, 1391.
(98) Benslimane, M.; Merazig, H.; Daran, J. C.; Zeghouan, O. Tris[4-(Dimethylamino)pyridinium][(Bis-μ-Dichlorido)-Decaaquadichloridodineodymium(III)] Pentachloride Dihydrate. *Acta Crystallogr., Sect. E: Struct. Rep. Online* **2012**, *68*, m1342−m1343.
(99) Zhongsheng, J.; Shenglong, W.; Fusong, W.; Cheng, S.; Guangdi, Y.; Yuguo, F. Experimental Crystal Structure Determination. *Gaodong Xuexiao Huaxue Xuebao* **1985**, *6*, 735.
(100) Clegg, W.; Harrington, R. W. Tetrakis(1,10-Phenanthrolinium) Hexachloridoeuropate(III) Chloride. *Acta Crystallogr., Sect. E: Struct. Rep. Online* **2007**, *63*, m1152.
(101) Hallfeldt, J. *CCDC 225125. Experimental crystal structure determination* 2004.
(102) Bailey, M. D.; Jin, G. X.; Ward, C. L.; Allen, M. J. *CCDC 2072184: Experimental Crystal Structure Determination; Cambridge Crystal Structural Database*, 2021.
(103) Shan, C. J.; Lin, Y. H.; Jin, S. C.; Ouyang, J.; Fan, Y. G.; Di, Y. G.; Yu, J. S. Single crystal structure of [Al~3Nd~6(M~2-Cl)~6-(M~3-Cl)~6(M~2-Et)~9Et~5OCH(CH~3)~2]~2. *Acta Chim. Sin.* **1987**, *45*, 949−954.
(104) Wen, J. W.; Chen, W. T.; Zhang, Z. X.; Tao, W. J.; Liu, C. The Mixed-Ligand Strategy to Assemble a Europium Metal-Organic Framework with a 2-Fold-Interpenetrated Network. *J. Solid State Chem.* **2018**, *263*, 30−35.
(105) Binnemans, K. Interpretation of Europium(III) Spectra. *Coord. Chem. Rev.* **2015**, *295*, 1−45.
(106) Yadav, A.; Pandey, S. Densities and Viscosities of (Choline Chloride + Urea) Deep Eutectic Solvent and Its Aqueous Mixtures in the Temperature Range 293.15 K to 363.15 K. *J. Chem. Eng. Data* **2014**, *59*, 2221−2229.
(107) Alcalde, R.; Atilhan, M.; Aparicio, S. On the Properties of (Choline Chloride + lactic Acid) Deep Eutectic Solvent with Methanol Mixtures. *J. Mol. Liq.* **2018**, *272*, 815−820.
(108) Housecroft, C. E.; Sharpe, A. G. *Inorganic Chemistry*, 4th ed.; Pearson Education limited: Harlow, 2012.
(109) Muetterties, E. L.; Wright, C. M. Molecular Polyhedra of High Co-Ordination Number. *Q. Rev. Chem. Soc.* **1967**, *21*, 109−194.
(110) Binnemans, K.; Görller-Walrand, C. Application of the Eu3+ Ion for Site Symmetry Determination. *J. Rare Earths* **1996**, *14*, 179−180.
(111) Bryden, C. C.; Reilley, C. N. Europium Luminescence Lifetimes and Spectra for Evaluation of 11 Europium Complexes as Aqueous Shift Reagents for Nuclear Magnetic Resonance Spectrometry. *Anal. Chem.* **1982**, *54*, 610−615.
(112) Albin, M.; Horrocks, W. D. W.; Liotta, F. J. Characterization of a Potentially Axially Symmetric Europium(III) Complex of a Tetraacetate,Tetraaza, Macrocyclic Ligand by Luminescence Excitation, Emission and Lifetime Spectroscopy. *Chem. Phys. Lett.* **1982**, *85*, 61−64.
(113) Jung, E. C.; Bae, S.; Park, Y. J.; Song, K. Time-Resolved Laser-Induced Fluorescence Spectroscopy of Nd 3 + in Molten LiCl − KCl Eutectic. *Chem. Phys. Lett.* **2011**, *516*, 177−181.
(114) Blasse, G.; Bril, A. On the Eu3+ Fluorescence in Mixed Metal Oxides. V. the Eu 3+ Fluorescence in the Rocksalt Lattice. *J. Chem. Phys.* **1966**, *45*, 3327−3332.
(115) Maia Melo, S.; Maria Câmara Jatahy, L.; Castellano, E. E.; Santos, C. O. P. Synthesis and Optical Study of Ln(III)-(Tetramethylurea)(AsF6)3 (Ln = LaLu, Y) and Crystal Structure for Ln = Eu [Eu(TMU)6(AsF6)3]. *Inorg. Chim. Acta* **1985**, *109*, 163−166.
(116) Thompson, L. C.; Kuo, S. C. Orange Luminescence from Europium(III) Compounds. *Inorg. Chim. Acta* **1988**, *149*, 305−306.
(117) Fujihara, S.; Oikawa, M. Structure and Luminescent Properties of CeO2:Rare Earth RE=Eu3+ and Sm3+ Thin Films. *J. Appl. Phys.* **2004**, *95*, 8002−8006.
(118) Eliseeva, S. V.; Bünzli, J. C. G. Lanthanide Luminescence for Functional Materials and Bio-Sciences. *Chem. Soc. Rev.* **2010**, *39*, 189−227.

https://doi.org/10.1021/acsomega.1c05386
ACS Omega 2022, 7, 921−932